Acta Pharmaceutica Sinica B 2023;13(5):2138–2151

Chinese Pharmaceutical Association
Institute of Materia Medica, Chinese Academy of Medical Sciences

Acta Pharmaceutica Sinica B

www.elsevier.com/locate/apsb
www.sciencedirect.com

ORIGINAL ARTICLE

Discovery and identification of EIF2AK2 as a direct key target of berberine for anti-inflammatory effects

Wei Wei[†], Qingxuan Zeng[†], Yan Wang[†], Xixi Guo, Tianyun Fan, Yinghong Li, Hongbin Deng, Liping Zhao, Xintong Zhang, Yonghua Liu, Yulong Shi, Jingyang Zhu, Xican Ma, Yanxiang Wang[*], Jiandong Jiang[*], Danqing Song[*]

Institute of Medicinal Biotechnology, Chinese Academy of Medical Sciences and Peking Union Medical College, Beijing 100050, China

Received 6 September 2022; received in revised form 5 November 2022; accepted 6 December 2022

KEY WORDS

Berberine;
Anti-inflammatory;
Target identification;
Chemoproteomic technology;
Photoaffinity probe;
EIF2AK2

Abstract Using chemoproteomic techniques, we first identified EIF2AK2, eEF1A1, PRDX3 and VPS4B as direct targets of berberine (BBR) for its synergistically anti-inflammatory effects. Of them, BBR has the strongest affinity with EIF2AK2 *via* two ionic bonds, and regulates several key inflammatory pathways through EIF2AK2, indicating the dominant role of EIF2AK2. Also, BBR could subtly inhibit the dimerization of EIF2AK2, rather than its enzyme activity, to selectively modulate its downstream pathways including JNK, NF-κB, AKT and NLRP3, with an advantage of good safety profile. In EIF2AK2 gene knockdown mice, the inhibitory IL-1β, IL-6, IL-18 and TNF-α secretion of BBR was obviously attenuated, confirming an EIF2AK2-dependent anti-inflammatory efficacy. The results highlight the BBR's network mechanism on anti-inflammatory effects in which EIF2AK2 is a key target, and inhibition of EIF2AK2 dimerization has a potential to be a therapeutic strategy against inflammation-related disorders.

*Corresponding authors.
E-mail addresses: wangyanxiang@imb.pumc.edu.cn (Yanxiang Wang), jiang.jdong@163.com (Jiandong Jiang), songdanqingsdq@hotmail.com (Danqing Song).
[†]These authors made equal contributions to this work.

Peer review under the responsibility of Chinese Pharmaceutical Association and Institute of Materia Medica, Chinese Academy of Medical Sciences.

https://doi.org/10.1016/j.apsb.2022.12.009

1. Introduction

During the past 20 years, more and more new biological effects of berberine (BBR, Fig. 1A), a natural antimalarial drug in China, have been gradually discovered and elucidated, such as type 2 diabetes, hyperlipidemia, atherosclerosis, and Alzheimer's disease[1−4]. Though its several direct proteomic targets, including ubiquitin-like with PHD and ring finger domains 1 (UHRF1), retinoid X receptor alpha (RXRα) and ephrin-B2, as well as NIMA-related kinase 7 (NEK7) and mitogen-activated protein kinase 7 (MKK7) recently reported by our group, have been identified[5−11], the complex and ingenious network mechanism of BBR has not been fully clarified. It is also unclear which proteins are the key targets that simultaneously regulate multiple signaling pathways, and how the key proteins play a more dominant role. If the key targets of BBR can be illuminated, it not only helps us understand the nature of biological evolution, but also provides the druggable targets for new drug discovery, worthy of further investigation.

Based on our previous research, we continued to search for the key direct targets against inflammation through activity-based proteome profiling (ABPP) techniques[9,12−15], using new BBR diphenyl-ketone photoaffinity probes. We first captured and identified the eukaryotic translation initiation factor 2 alpha kinase 2 (EIF2AK2, also known as PKR), eukaryotic translation elongation factor 1 alpha 1 (eEF1A1), peroxiredoxin 3 (PRDX3) and vacuolar protein sorting 4 homolog B (VPS4B) as direct targets of BBR for its synergistically anti-inflammatory effects, through *in vitro* binding assays and orthogonal confirmatory experiments. Among these four proteins, BBR strongly binds to EIF2AK2 *via*

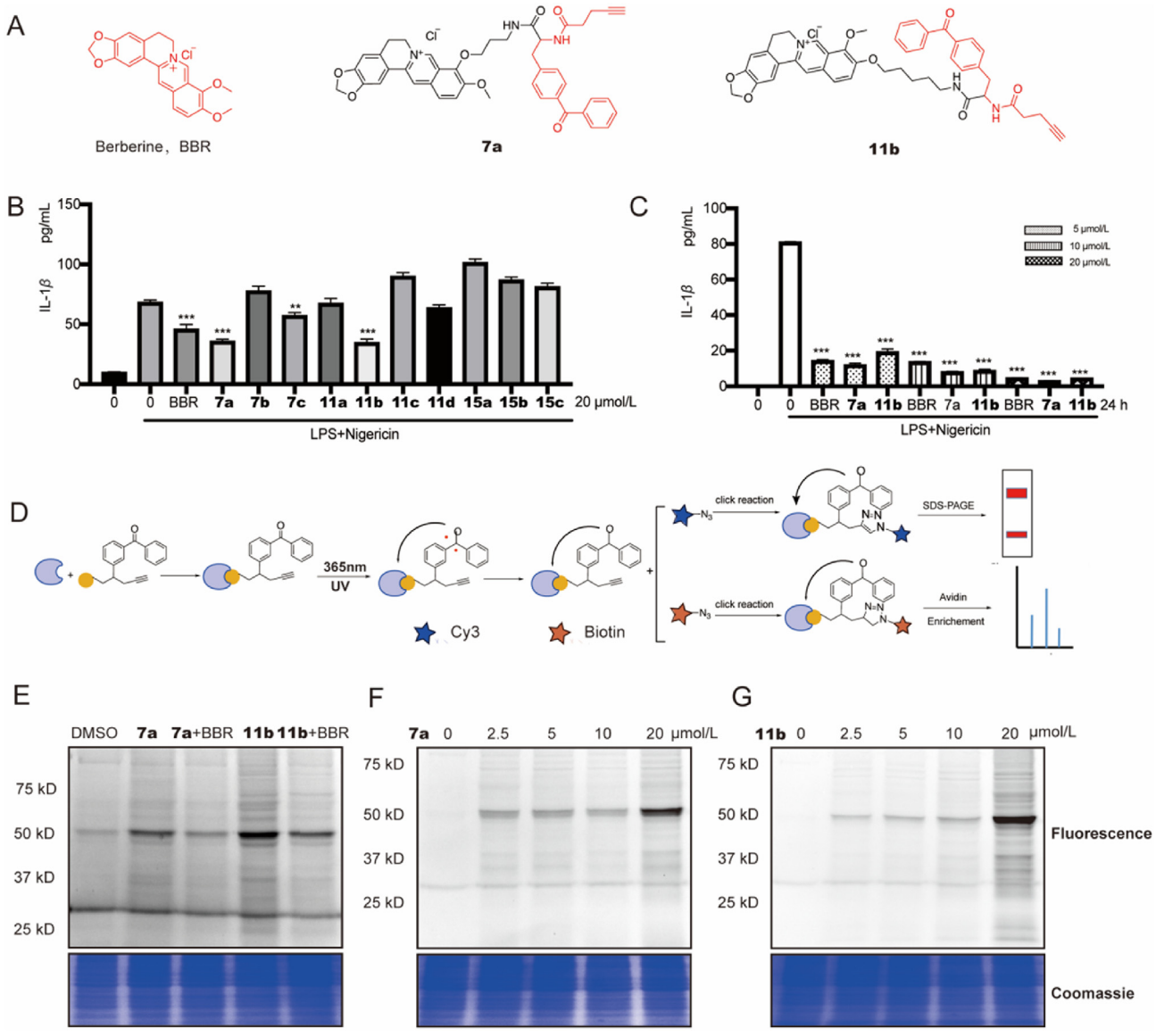

Figure 1 Screening and evaluation of BBR probes. (A) The structures of BBR, **7a** and **11b**. (B, C) ELISA analysis of cleaved IL-1β in culture supernatants. THP-1 cells were primed with LPS and then stimulated with nigericin, with BBR or all probes (20 μmol/L) pretreatment for 24 h (B), with BBR, **7a** or **11b** at different concentrations (C). (D) The whole process of target capture and identification. (E−G) PMA-THP-1 cells were incubated with 10 μmol/L **7a** and **11b** for 6 h with or without BBR (100 μmol/L) pretreatment for 3 h (E), or incubated with different concentrations of **7a** (F) or **11b** (G) for 6 h. Followed by 365 nm light exposure, the proteome was coupled with Cy3 and separated by SDS-PAGE.

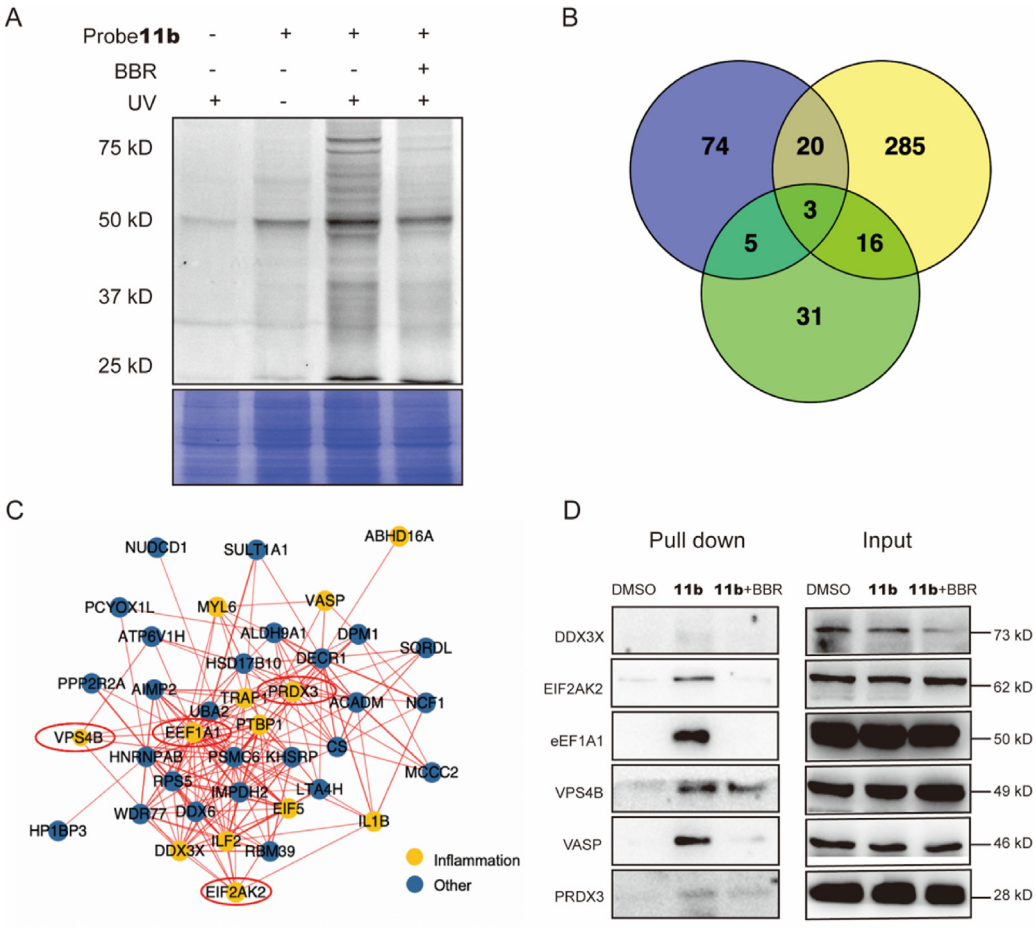

Figure 2 Target proteins capture and functional analysis. (A) PMA-THP-1 cells were incubated with 10 μmol/L **11b** for 6 h with or without BBR (100 μmol/L) pretreated for 3 h. Followed by 365 nm light exposure or not, the labeled proteome was clicked by Cy3 and separated by SDS-PAGE. (B) Venn diagram analysis, the number of proteins with the quantified ratio ≥2.0 identified in each set of ABPP experiments. (C) Protein interaction analysis of captured proteins. (D) Captured targets were verified by immunoblot assay using the probe **11b** pulling down. Competitive inhibition was performed using 100 μmol/L BBR.

ionic bonds with the K_d value of 7.12 μmol/L, and simultaneously regulates multiple inflammatory pathways through EIF2AK2, suggesting that EIF2AK2 serves as a key target of BBR for anti-inflammatory potency. Furthermore, BBR could subtly inhibit the dimerization rather than enzymatic activity to selectively suppress multiple inflammatory signaling pathways, such as c-Jun *N*-terminal kinase (JNK), nuclear factor kappa-light-chain-enhancer of activated B cells (NF-κB), protein kinase B (AKT) and nod-like receptor protein 3 (NLRP3), with an advantage of good safety profile. The *in vivo* study further confirms that BBR suppresses inflammation reactions in an EIF2AK2-dependent manner. Our data demonstrate that EIF2AK2 acts as a key target of BBR to regulate multiple signaling pathways, enabling BBR to synergistically perform anti-inflammatory efficacies.

2. Results

2.1. *Fluorescence labelling of BBR targets in THP-1 cells*

A series of new BBR photoaffinity probes with diphenyl-ketone as a photo cross-linking group (**7a**−**c**, **11a**−**d**, **15a**−**c**, Supporting Information Fig. S4) were synthesized and evaluated for their activities against several inflammatory factors in PMA (phorbol 12-myristate-13-acetate)-differentiated THP-1 (human monocytic cell line-1) cells (PMA-THP-1) triggered by LPS plus nigericin[16−20]. As shown in Fig. 1A−C and Fig. S4, probes **7a** and **11b** exhibited better potencies on interleukin-1β (IL-1β) suppression in a time- or dose-dependent manner, better than that of BBR. The suppressive potencies were further confirmed (Supporting Information Figs. S5 and S6) on IL-6, IL-8, and monocyte chemoattractant protein-1 (MCP-1), and then both probes were used for the next step.

The overall process of target capture and identification using ABPP assay is presented in Fig. 1D. Firstly, both **7a** and **11b** (10 μmol/L) were incubated with PMA-THP-1 cells to profile the direct target proteins of BBR *in situ*. Followed by 365 nm light exposure, the highly active diphenyl-ketone free radicals rapidly generated and covalently bond to the hydroxyl groups or α-hydrogen atoms of the captured target proteins[21,22]. After being clicked with Cy3-azide and resolved by SDS-polyacrylamide gel electrophoresis (SDS-PAGE), bound targets of **7a** and **11b** can be labelled and visualized with fluorescence scanning, which could be competitively inhibited by BBR (100 μmol/L, Fig. 1E), indicating a similar mechanism of action to BBR. More significant changes in fluorescence intensity were observed in probe **11b** treatment group at the concentrations ranging from 2.5 to

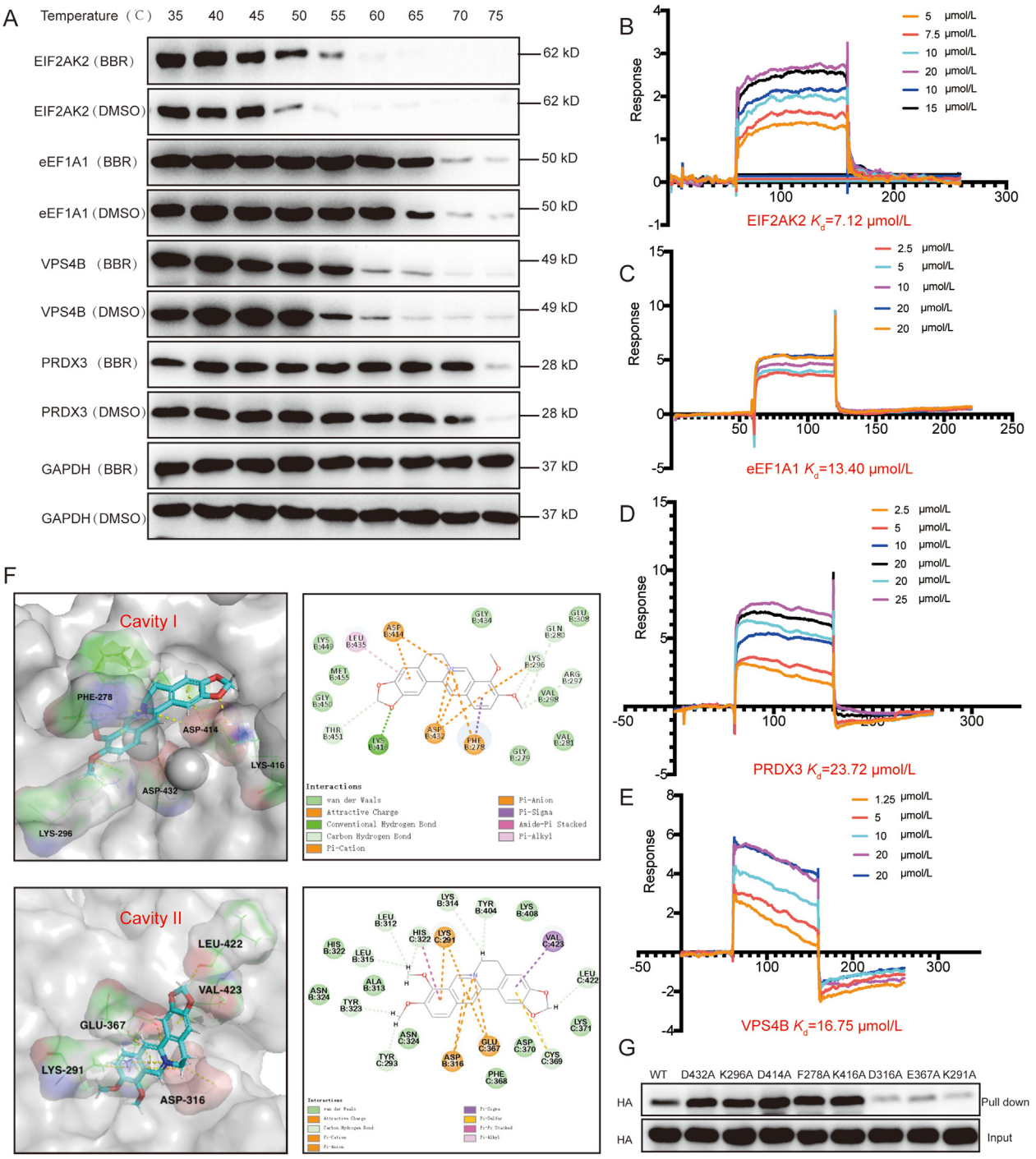

Figure 3 Affinity studies between BBR and its potential targets. (A) The thermal stabilities of the proteins with or without BBR. (B−E) SPR assay obtained separately on EIF2AK2-coated, eEFF1A1-coated, PRDX3-coated and VPS4B-coated chip in the presence of different concentrations of BBR. (F) Molecular docking results for EIF2AK2 (PDB code: 2A19) with BBR. (G) WT or mutant EIF2AK2 was pulled down with **11b** and analyzed by immunoblotting.

20 μmol/L (Fig. 1F and G), and it was chosen as a functional probe for the next chemoproteomic profiling.

2.2. *Identification of BBR target*

Next, PMA-THP-1 cells were incubated with **11b** (10 μmol/L) for 6 h with or without BBR (100 μmol/L) pretreated for 3 h, taking DMSO as the control. Followed by 365 nm light exposure, the labeled proteome was linked with Cy3 and separated by SDS-PAGE. As shown in Fig. 2A, and fluorescence intensity of several different bands with the molecular weights (MW) between 25 and 80 kDa were detected. Compared with the **11b** group, the fluorescent bands under the UV (365 nm) exposure were obviously enhanced, owing to covalently capturing the target proteins

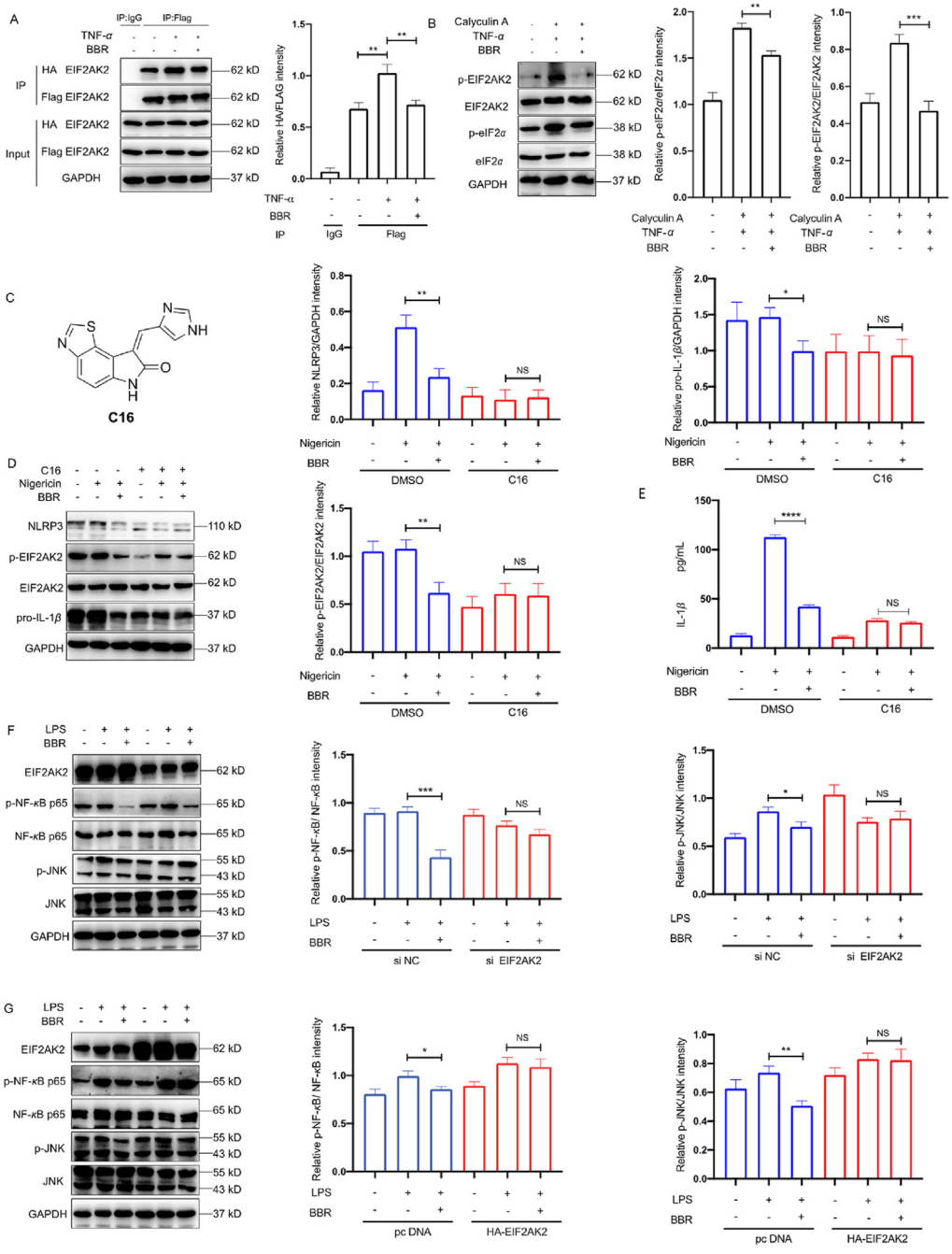

Figure 4 (*continued on next page*).

of **11b**. The labeled bands were distinctly attenuated followed by an addition of BBR, which again verified the specific labeling capacity of **11b**.

Then the labeled proteins were coupled with biotin−azide, **11b**−biotin complexes were formed and purified by streptavidin magnetic beads and identified with LC−MS/MS analysis. The quantitative ratio of proteome in group **11b/11b** plus BBR reflects the extent of competition by the native BBR, with a larger ratio corresponding to greater competition. The DMSO control group was set to eliminate false-positive targets resulting from nonspecific binding to the beads. Three replicates were performed for each of the control and competition experiments with a cutoff of 2.0 for the quantified ratio analysis. We collectively identified 44 proteins between 20 and 80 kDa as potential targets, which appeared in the protein list twice or more (Fig. 2B and Supporting Information Table S2).

Gene Ontology (GO) enrichment indicated that the 44 proteins were closely involved in various inflammatory signaling pathways (Supporting Information Figs. S7A and B), of which 13 (yellow dots in Fig. 2C) were inflammation-related proteins through protein interaction analysis. By analyzing the comprehensive function and involved pathways of these proteins, six proteins, including EIF2AK2, eEF1A1, PRDX3, DEAD-box helicase 3 X-linked (DDX3X), Vasodilator stimulated phosphoprotein (VASP) and

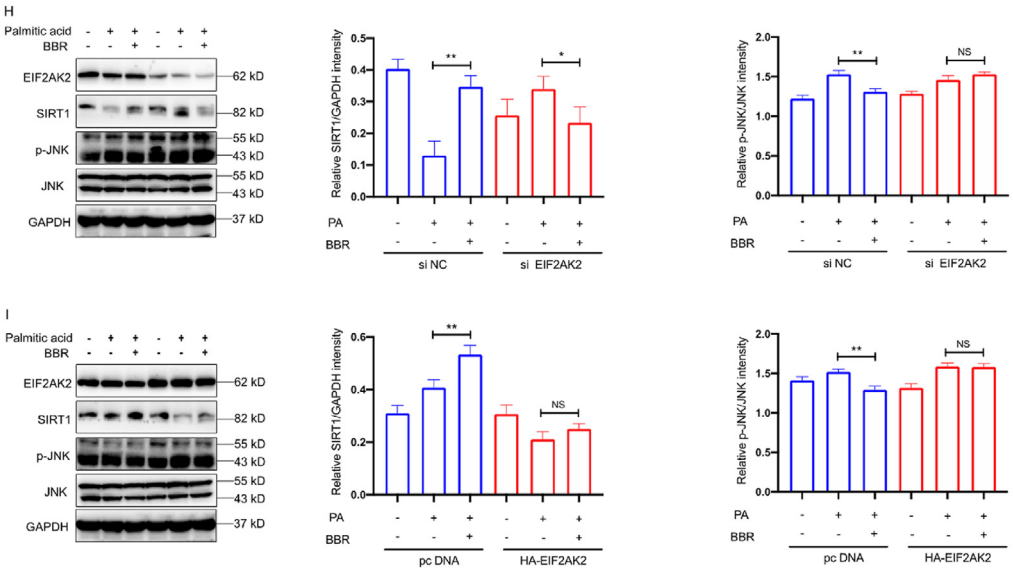

Figure 4 Functional studies of EIF2AK2. (A) BBR inhibits EIF2AK2 dimerization using immunoprecipitation assay. (B) HEK-293 cells were treated with calyculin A for 10 min, then cells were stimulated with TNF-α for 15 min, with or without BBR pretreatment for 6 h. (C) The structure of C16. (D, E) PMA-THP-1 cells were primed with LPS and then stimulated with nigericin, with or without BBR/C16 pre-treatment for 24 h. Immunoblot analysis of NLRP3 in lysates (D) and ELISA analysis of cleaved IL-1β in culture supernatants (E). (F, G) Immunoblot analysis of indicated protein level. HMC3 cells were transfected with EIF2AK2 siRNA (F) or EIF2AK2 plasmid (G) for 48 h, then cells were stimulated by LPS for 4 h, with or without BBR pretreatment for 6 h. (H, I) Immunoblot analysis of indicated protein level. HepG2 cells were transfected with EIF2AK2 siRNA (H) or EIF2AK2 plasmid (I) for 24 h, then cells were stimulated by PA for 24 h, with or without BBR pretreatment for 2 h ($n = 3$). Data are presented as mean ± SD, $^*P < 0.05$; $^{**}P < 0.01$, $^{***}P < 0.001$, NS, no significant.

VPS4B, were closely related to BBR's indications[23−27]. Also, these six proteins could regulate two or more inflammatory pathways and have the potential to play a key role in BBR's anti-inflammatory potency[28−36]. More recently, we have demonstrated the important role of VASP in BBR's antiplatelet aggregation[37], and thus other five proteins were selected for the further investigation. Of the five proteins, except for DDX3X, the EIF2AK2, eEF1A1, PRDX3 and VPS4B were successfully confirmed to be the potential direct target proteins of BBR by immunoblot assay using the active probe **11b** pulling down (Fig. 2F). Obvious competitive inhibition could be detected while 100 μmol/L BBR was pre-treated, indicating the possible specific interactions between BBR and these four proteins.

Then, CETSA experiment was performed in HEK-293 cells to verify the interaction between BBR and the four target proteins. The thermal stability of EIF2AK2, eEF1A1, PRDX3 and VPS4B was enhanced in different degrees with the addition of BBR (10 μmol/L) ranging from 35 to 75 °C (Fig. 3A), indicating possible direct interactions between BBR and these four proteins. Among them, BBR showed minor interactions with eEF1A1 and PRDX3, which may be due to the strong thermal stability in 55 to 65 °C temperature range of these two proteins. Subsequently, SPR analysis was conducted using the recombinant proteins for further confirmation, and the K_d values of BBR with EIF2AK2, eEF1A1, PRDX3 and VPS4B were 7.12, 13.4, 23.7 and 16.8 μmol/L (Fig. 3B−E), respectively. Furthermore, molecular docking between BBR and the four proteins was carried out using Discovery Studio 4.5 software, and docking scores were respectively 100.2, 88.8, 86.7 and 91.6, basically consistent with the affinity values (Fig. 3F, Supporting Information Figs. S8−S10). These results again verified the specific interactions between BBR and these four target proteins, in which BBR had the strongest affinity with EIF2AK2.

Meanwhile, EIF2AK2 can modulate multiple signal transduction pathways, and is responsible for several inflammation-related diseases, such as virus-infections, glucose/lipid metabolism disorders and neuro-inflammations[25,27,38−40]. These results suggested that EIF2AK2 might play a more dominant role than other three proteins, and thus we conducted in-depth study on the interaction pattern with BBR and the anti-inflammation function of EIF2AK2.

2.3. *Binding pattern of BBR with EIF2AK2*

Based on the strong affinity between BBR and EIF2AK2, it is speculated that there may be ionic bonds between them. Then, two cavities containing different ionic-bond interactions were selected to conduct molecular docking using Discovery Studio 4.5 software. Eight key amino acid residues, including D432, K296, D414, F278, K416 in Cavity I (Fig. 3F, upper row), and D316, E367, K291 in Cavity II (Fig. 3F, lower row), are potential to play the key roles. The single-point mutation of the eight residues was carried out one by one to identify the binding sites of EIF2AK2. All eight residues in sequence were respectively converted into alanine (A) that cannot easily interact with its substrate (Fig. 3F), and only the mutations of D316, E367 and K291 in Cavity II significantly abolished the binding affinity between BBR and EIF2AK2 (Fig. 3G). The results indicated that BBR could act on EIF2AK2 mainly through two ionic bonds with D316 and E367 and one Pi−cation bond with K291 in Cavity II. Of note, this cavity is precisely involved in the dimerization of EIF2AK2 (Fig. 3F), which is responsible for the downstream cascade inflammation-related reactions[39,40], suggesting that BBR might directly target dimerization of EIF2AK2 to regulate the anti-inflammatory effects.

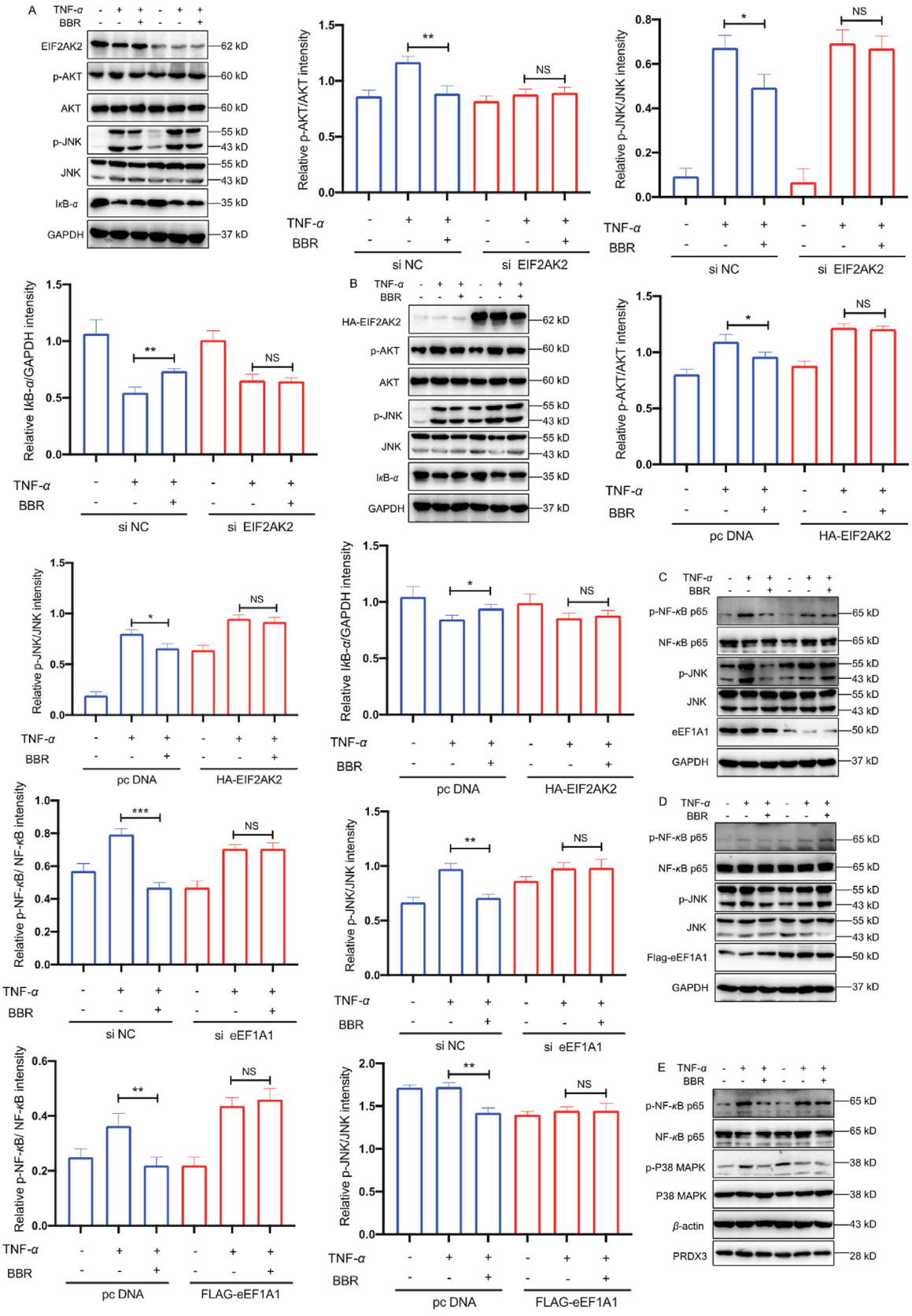

Figure 5 (*continued on next page*).

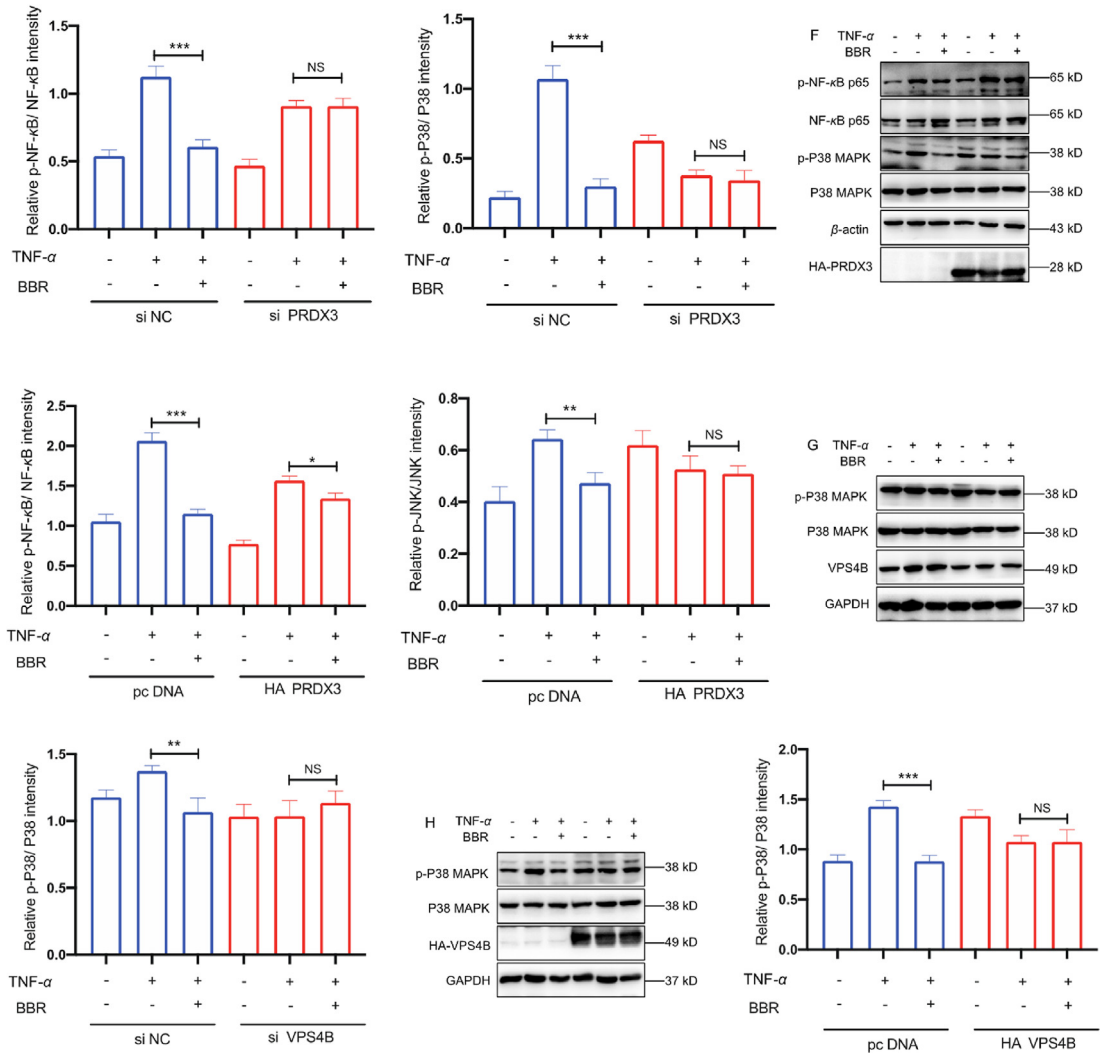

Figure 5 Functional studies of BBR targets. (A, B) Immunoblot analysis of indicated protein level. HEK-293 cells were transfected with EIF2AK2 siRNA (A) or EIF2AK2 plasmid (B) for 48 h, then cells were stimulated by TNF-α for 15 min, with or without BBR pretreatment for 6 h. (C, D) Immunoblot analysis of indicated protein level. HEK-293 cells were transfected with eEF1A1 siRNA (C) or eEF1A1 plasmid (D) for 48 h, then cells were stimulated by TNF-α for 15 min, with or without BBR pretreatment for 6 h. (E, F) Immunoblot analysis of indicated protein level. HEK-293 cells were transfected with PRDX3 siRNA (E) or PRDX3 plasmid (F) for 48 h, then cells were stimulated by TNF-α for 15 min, with or without BBR pretreatment for 6 h. (G, H) Immunoblot analysis of indicated protein level. HEK-293 cells were transfected with VPS4B siRNA (G) or VPS4B plasmid (H) for 48 h, then cells were stimulated by TNF-α for 15 min, with or without BBR pretreatment for 6 h. $n = 3$, Data are presented as mean ± SD, $^{*}P < 0.05$; $^{**}P < 0.01$, $^{***}P < 0.001$, NS, no significant.

Then, we used an immunoprecipitation approach to further verify if BBR interferes with EIF2AK2 dimerization. HEK-293 cells were cotransfected with plasmids expressing both HA-tagged EIF2AK2 and FLAG-tagged EIF2AK2 to conveniently observe dimerization behavior. The cells were treated with TNF-α for 15 min before lysed to trigger EIF2AK2 dimerization, and then subjected to immunoprecipitation using anti-FLAG magnetic beads. As shown in Fig. 4A, HA- and FLAG-tagged EIF2AK2 were dimerized in the control experiment, which was significantly promoted after TNF-α treatment, and BBR dramatically decreased the level of dimerization between HA- and FLAG-tagged EIF2AK2, demonstrating that BBR inhibited dimerization interaction of EIF2AK2. Since autophosphorylation happens after EIF2AK2 dimerization[39,41,42], the effect of BBR on EIF2AK2 autophosphorylation was carried out. As depicted in Fig. 4B, followed by suppression of EIF2AK2 dimerization, BBR significantly inhibited the EIF2AK2 autophosphorylation on residues Thr446[40], as well as EIF2AK2 substrate eIF2α phosphorylation, further indicating that BBR affected the downstream functions by acting on EIF2AK2 dimerization.

Directly targeting EIF2AK2 dimerization or its autophosphorylation might lead to different down-stream effect. To further understand this difference, EIF2AK2 autophosphorylation inhibitor C16 (Fig. 5C) was chosen for the determination of activities on EIF2AK2 inhibition. Half maximal inhibitory concentration (IC_{50}) of BBR and C16 was respectively 50.0 and 1.01 μmol/L (Supporting Information Fig. S11). Meanwhile, 50% cytotoxity concentration (CC_{50}) of both was also tested and calculated in THP-1 cells. BBR showed a moderate cytotoxicity with a CC_{50} value of 91.4 μmol/L, much higher than that of C16 with CC_{50} of

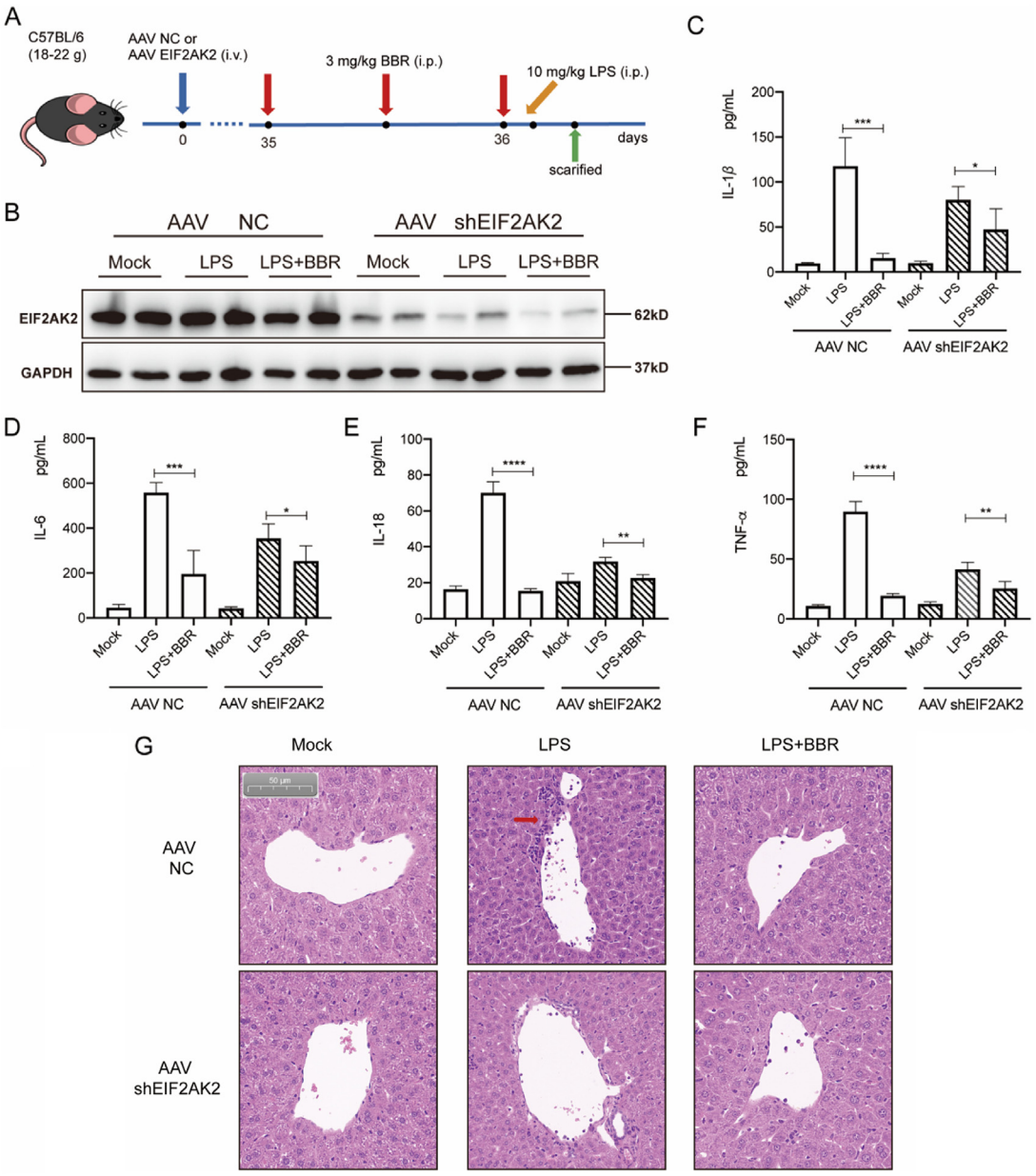

Figure 6 EIF2AK2 functional verifications *in vivo*. (A) Mice transfected with AAV for 35 days and treated with BBR two times every 12 h before LPS stimulation. (B) Immunoblot analysis of EIF2AK2 expression in mouse livers. (C) ELISA analysis of IL-1β in mouse serum. (D) ELISA analysis of IL-6 in mouse serum. (E) ELISA analysis of IL-18 in mouse serum. (F) ELISA analysis of TNF-α in mouse serum. (G) Representative H&E staining of liver sections of mice ($n = 5$). Data are presented as mean ± SD, $^{*}P < 0.05$; $^{**}P < 0.01$, $^{***}P < 0.001$.

1.13 μmol/L (Fig. S11). These results suggested that BBR could avoid possible toxicities by targeting EIF2AK2 dimerization to selectively exert related activities, which provided a possible explanation for its good safety profile of BBR.

2.4. *Functional studies of EIF2AK2*

To further understand the functional effect of EIF2AK2, we first validated the function of NLRP3 inflammasome by measuring IL-1β release in PMA-THP-1 cells. BBR (10 μmol/L) inhibits the expression of NLRP3 and then blocks the downstream IL-1β release, while EIF2AK2 was pharmacologically inhibited by its inhibitor C16, such reductions in NLRP3 expression and IL-1β release were not observed (Fig. 5D and E)[43,44], which indicated that BBR might suppress NLRP3 expression and IL-1β release through acting on EIF2AK2.

As EIF2AK2 is relatively high-expressed in brain tissue[41,45,46], we further verified the correlation between EIF2AK2 and the inflammatory pathways in human-derived microglia (HMC3) cells. As expected, BBR could down-regulate p-NF-κB p65 and p-JNK induced by LPS (Fig. 5F and G), while the effect of BBR on suppressing p-NF-κB p65 and p-JNK was lost partially or completely after EIF2AK2 was knocked down. Furthermore, when EIF2AK2 was overexpressed, the BBR-dependent inhibition

of p-NF-κB p65 was reversed and p-JNK was attenuated. These results hinted that BBR could affect cerebral inflammatory reactions through targeting EIF2AK2, and provided a possible mechanism how BBR exerted anti-inflammatory related diseases in the brain, such as gliosis and cognitive impairment in Alzheimer's disease[41,45,47,48].

In addition, EIF2AK2 acts as a key signaling protein in fatty acid-induced ER stress to bridge the signals between lipid metabolism and inflammation through promoting JNK activation, followed by down-regulating NAD-dependent protein deacetylase sirtuin-1 (SIRT1) expression[49,50], among which SIRT1 is an important biomarker closely related to lipid metabolism. As shown Fig. 5H and I, BBR could inhibit the level of p-JNK induced by palmitic acid (PA) and up-regulate the expression of SIRT1 protein in HepG2 cells. Knocking down or overexpression EIF2AK2 significantly neutralized the decreasing p-JNK level and increasing expression of SIRT1 mediated by BBR, compared with wild type cells. The results further demonstrated that BBR may regulate inflammation-induced lipid metabolism disorders through binding to the key protein EIF2AK2.

2.5. *Functional studies of four BBR targets*

Furthermore, we selected the classic inflammation-related pathways each protein involved for their functional verification. Overexpressing or knock-down models of the four proteins at cellular level were established to investigate whether BBR could regulate different classical inflammatory pathways in a dependent manner, such as JNK, NF-κB, mitogen-activated protein kinase (MAPK) and AKT signals.

Firstly, in HEK-293 cells, BBR inhibits the degradation of IκBα protein, and the level of JNK phosphorylation (p-JNK) and p-AKT induced by tumor necrosis factor-α (TNF-α) (Fig. 5A and B). When EIF2AK2 was silenced by siRNA, the inhibitory effect of BBR on degradation of IκBα and p-AKT was abolished, while the BBR-dependent down-regulation of p-JNK was attenuated (Fig. 5A). Moreover, overexpression of EIF2AK2 also reversed the inhibitory effect of BBR (Fig. 5B) on IκBα degradation, p-JNK and p-AKT respectively[41]. Similarly, the regulatory effects of BBR on p-JNK and p-NF-κB p65 were attenuated in eEF1A1 overexpressing or knock-down models (Fig. 5C and D)[34,51]. Also, we have observed consistent results of BBR on p-NF-κB p65 and p-P38 MARK regulations, while PRDX3 was overexpressed or knocked down in HEK-293 cells (Fig. 5E and F)[28]. Finally, the decreased efficacy of BBR on p-P38 MARK signaling with VSP4B overexpressed or knocked down was observed (Fig. 5G and H)[35]. These results indicated that BBR modulates multiple signaling pathways including JNK, NF-κB, MAPK and AKT, through EIF2AK2, eEF1A1, PRDX3 and VPS4B dependent manners respectively, among which EIF2AK2 plays a dominant role, and then *in vivo* experiment was conducted for further confirmation.

2.6. *Anti-inflammatory efficacy in EIF2AK2 knockdown mice*

It is known that IL-1β, IL-6, IL-18 and TNF-α secretions are closely linked to several factors, such as inflammasome NLRP3 expression, and activations of JNK and NF-κB pathways[52–55], and then we further demonstrated whether BBR affects IL-1β, IL-6, IL-18 and TNF-α release by targeting EIF2AK2 *in vivo*. Thus, an EIF2AK2 knockdown mouse model was successfully established by 35 days of intravenous injection of adeno-associated virus (AAV) shEIF2AK2 in mice to evaluate the effects of BBR on IL-1β, IL-6, IL-18 and TNF-α (Fig. 6A), the expression of EIF2AK2 was significantly decreased compared with the control group (Fig. 6B). Then, wild type mice and EIF2AK2 knockdown mice were respectively injected with BBR twice at 24 h intervals *via* intraperitoneal injection (i.p.) at a dose of 3 mg/kg, and then LPS was administrated. BBR significantly reduced the production of IL-1β, IL-6, IL-18 and TNF-α in the control group (Fig. 6B–F), while the effect of BBR was partly weakened in the EIF2AK2 gene knockdown group,

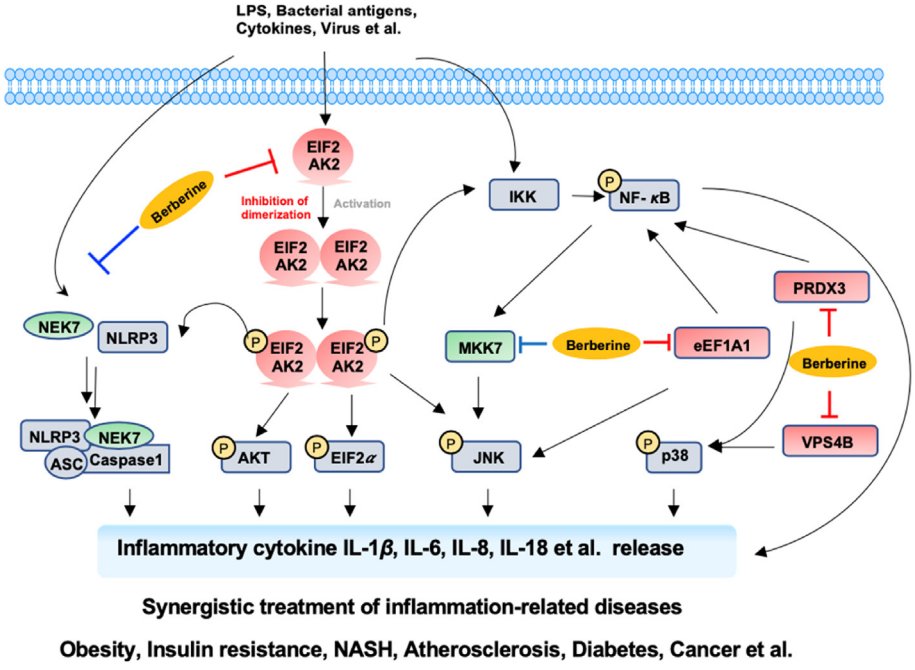

Figure 7 Cartoon of BBR's anti-inflammatory mechanism.

indicating the EIF2AK2-relevant effect of BBR on IL-1β, IL-6, IL-18 and TNF-α. H&E staining of liver results (Fig. 6G) showed that the alleviation on inflammatory infiltration of liver by BBR was weakened in the EIF2AK2 gene knockdown mice. No significant lesions were found in other tissues (Supporting Information Fig. S12), consistent with the above conclusions. These results demonstrated that BBR might downregulate IL-1β, IL-6, IL-18 and TNF-α secretions *via* targeting EIF2AK2 with a good safety profile.

3. Conclusions

Since ionic bond is the strongest noncovalent bond, we consider that BBR owns the strongest binding force with EIF2AK2 *via* two ionic bonds. Meanwhile, EIF2AK2 modulates multiple signal transduction pathways, including AKT, JNK and NF-κB pathways in an EIF2AK2-dependent manner. Therefore, among the four newly identified direct targets of BBR for anti-inflammatory effects, including EIF2AK2, eEF1A1, PRDX3 and VPS4B, EIF2AK2 serves as a key target to treat several inflammation related diseases. Combining NEK7 and MKK7 recently reported by our group, BBR also directly targets EIF2AK2, eEF1A1, PRDX3 and VPS4B, to synergistically alleviate downstream inflammatory response and cytokines release, and the net mechanism of BBR's anti-inflammatory action was outlined as shown in Fig. 7. Since BBR exerts its diverse pharmacological activities through a multi-target network mechanism, it is necessary to further explore more direct targets and clarify the contribution of each target, in order to fully elucidate the complex and ingenious network mechanism, as well as the corresponding biological effects.

In addition, the dimerization of EIF2AK2 followed by auto-phosphorylation leads to the full catalytic activation, which can trigger lots of typical inflammatory pathways and inflammation related diseases, such as virus-infections, glucose/lipid metabolism disorders and neuroinflammations[41,42]. Different from C16 targeting EIF2AK2 enzyme activity, BBR directly inhibits the dimerization of EIF2AK2 to exert synergistic anti-inflammatory effects with an advantage of good safety profile. Thus, inhibition of EIF2AK2 dimerization may be developed into an important therapeutic target for inflammation-related diseases.

4. Experimental

4.1. Cell preparation and stimulation

Along with 10% FBS, DMEM was used for HEK-293 and HepG2 cells culture. RPMI with 10% FBS was applied for THP-1 cells culture. After 50 nmol/L PMA was added, THP-1 cells were differentiated for 1−2 days, before they were stimulated. Then, along with 10% FBS, HMC3 cells were cultured by MEM.

For induction of inflammasome activation, PMA-THP-1 cells were plated in 6-well plates, and primed for 3 h with ultrapure lipopolysaccharide (LPS, 1 μg/mL) with or without BBR pretreatment, then the cells were stimulated for 30 min with nigericin (5 μmol/L). The precipitated supernatants were analyzed by ELISA.

For stimulated classical inflammatory pathways, HEK-293 cells were plated in 6-well plates, and transfected with EIF2AK2 siRNA or EIF2AK2 plasmid for 48 h, then cells were stimulated by TNF-α for 15 min with or without BBR pretreatment for 6 h. The cell extracts were analyzed by immunoblot.

For stimulated neuro-inflammation, HMC3 cells were transfected with EIF2AK2 siRNA or EIF2AK2 plasmid for 48 h, then cells were stimulated by LPS for 4 h with or without and BBR pretreatment for 6 h. The cell extracts were analyzed by immunoblot.

For stimulated hepatocyte steatosis, HepG2 cells were transfected with EIF2AK2 siRNA or EIF2AK2 plasmid for 24 h, then cells were stimulated by PA for 24 h with or without BBR pretreatment for 2 h. The cell extracts were analyzed by immunoblot.

4.2. Chemical synthesis

The synthetic schemes and general procedures of **7a−c**, **11a−d** and **15a−c** were shown in Supporting Information Figs. S1−S3 and synthesis section, respectively.

Synthesis of **7a**. (3-(4-Benzoylphenyl)-1-(ethynylamino)-1-oxopropan-2-yl)carbamic acid (1.1 eq), EDCI (1.2 eq), HOBT (1.2 eq) and triethylamine (2.8 eq) were mixed in 5 mL DMF. After stirring for 1 h, compound **6a** was added and the mixture was stirred overnight. After the solvent was removed, the residue was purified through flash chromatography using CH_2Cl_2/CH_3OH to obtain **7a** as yellow solid, yield 41%; Mp: 89−91 °C; purity 96.7%; ^{1}H NMR (500 MHz, DMSO-d_6) δ 9.88 (s, 1H), 8.92 (s, 1H), 8.37 (d, J = 8.5 Hz, 1H), 8.11 (d, J = 9.0 Hz, 1H), 7.96 (d, J = 2.0 Hz, 1H), 7.85 (d, J = 8.5 Hz, 1H), 7.80 (s, 1H), 7.74−7.72 (m, 2H), 7.70−7.69 (m, 2H), 7.68 (s, 1H), 7.67−7.66 (m, 2H), 7.65−7.63 (m, 2H), 7.10 (s, 1H), 6.18 (s, 2H), 4.94−4.92 (m, 2H), 4.55−4.53 (m, 1H), 4.49−4.47 (m, 2H), 4.11 (s, 2H), 3.19−3.16 (m, 6H), 2.89 (s, 1H), 2.76−2.74 (m, 4H), 1.93−1.91 (m, 2H); ^{13}C NMR (126 MHz, DMSO-d_6) δ 196.2, 173.6, 170.8, 150.5, 150.2, 148.4, 146.0, 144.4, 143.8, 143.5, 137.8, 137.7, 135.8, 135.7, 133.3, 132.2, 130.3, 130.2, 130.1, 129.3, 129.2, 129.2, 128.4, 124.3, 122.0, 121.1, 120.9, 119.4, 109.1, 106.1, 102.8, 84.3, 72.0, 67.6, 62.6, 54.5, 53.9, 38.6, 37.5, 34.6, 29.5, 27.0, 14.7. HRMS: calcd for $C_{43}H_{40}N_3O_7Cl$ $[M-Cl]^+$ 710.2863, found 710.2861.

11b. Yield: 39%; Mp: 90−92 °C; purity 97.9%; ^{1}H NMR (500 MHz, DMSO-d_6) δ 9.87 (s, 1H), 8.92 (s, 1H), 8.31 (d, J = 8.5 Hz, 1H), 8.17 (d, J = 9.0 Hz, 1H), 8.10 (t, J = 5.5 Hz, 1H), 7.95 (d, J = 9.0 Hz, 1H), 7.85 (d, J = 8.5 Hz, 2H), 7.79 (s, 1H), 7.70 (d, J = 1.5 Hz, 2H), 7.68 (d, J = 3.5 Hz, 2H), 7.65 (d, J = 8.5 Hz, 2H), 7.62 (s, 1H), 7.09 (s, 1H), 6.18 (s, 2H), 4.92 (t, J = 6.5 Hz, 2H), 4.48 (d, J = 5.0 Hz, 1H), 4.25 (t, J = 6.5 Hz, 2H), 4.09 (s, 3H), 3.17 (m, 4H), 2.99 (m, 2H), 2.74 (d, J = 2.5 Hz, 1H), 2.28 (m, 4H), 1.80 (m, 2H), 1.43 (s, 2H), 1.23 (s, 2H); ^{13}C NMR (126 MHz, DMSO-d_6) δ 196.0, 170.7, 170.6, 150.3, 150.2, 148.2, 144.2, 143.7, 143.3, 137.9, 137.7, 135.6, 135.5, 133.4, 133.1, 131.1, 130.1, 130.0, 130.0, 129.9, 129.9, 129.9, 129.0, 129.0, 128.2, 124.1, 123.9, 119.2, 108.9, 105.9, 102.6, 84.1, 71.8, 69.9, 62.4, 55.6, 54.2, 38.8, 38.5, 34.4, 29.1, 28.9, 26.8, 23.2, 14.6. HRMS: calcd for $C_{45}H_{44}N_3O_7Cl$ $[M-Cl]^+$ 738.3176, found 738.3174.

4.3. Plasmid constructions

HA-EIF2AK2 plasmid was purchased from Sino Biological and gene mutation was performed using the QuikChange Lightning Site-Directed Mutagenesis Kit (Agilent). The protein expression EIF2AK2 (258−551 residues, H412N, C551A) was amplified by gene synthesis and inserted into PGEX-6P-1 vector. All primer sequences used are listed in Supporting Information Table S1.

4.4. In situ labeling in PMA-THP-1 cells

PMA-THP-1 cells were plated to 80%−90% confluence in 6-well plates, the medium was removed, and cells were washed twice

with PBS and then treated with 2 mL growth medium containing probe with or without BBR (100 μmol/L). After incubation at 37 °C/5% CO_2 for 3 h, the medium was aspirated, and cells were washed twice gently with PBS followed by UV irradiation (∼365 nm) for 30 min. The cells were then lysed by HEPES buffer (25 mmol/L HEPES, 150 mmol/L NaCl, 2 mmol/L $MgCl_2$) containing 1% NP-40, and the protein concentration was determined by Bradford protein assay (Bio-Rad USA). Equal amount sample with different treatment was used for fluorescent tagging or biotin tagging. For each click reaction, SDS (0.1%), TCEP (1 mmol/L), $CuSO_4$ (1 mmol/L), TBTA (100 μmol/L) and Cy3-azide or biotin-azide (100 μmol/L) was sequentially added to the lysates, and samples were incubated for 2 h, then the labeled proteins were precipitated with acetone. For fluorescence detection, the samples were dissolved with 1 × SDS loading buffer and boiled at 95 °C for 10 min. For LC−MS/MS and immunoblot detection, the samples were dissolved in HEPES buffer with 1% SDS, and incubated with washed beads for 2 h. After washed 5 times with TBS-T, the beads were mixed with 1 × SDS loading buffer, followed by boiling at 95 °C for 10 min. Samples were detected by gel fluorescence or immunoblot blot assay (Tanon 5200 system, Tanon, Shanghai, China).

4.5. Liquid chromatography tandem mass spectrometry (LC−MS/MS)

The proteome after 95 °C boiling to release from beads and identified with a label-free based LC−MS/MS approach (Beijing Qinglian Biotech Co., Ltd., China). MS was analyzed using Maxquant software (version 1.5.3.30) with the UniProtKB/Swiss-Prot human database.

4.6. Cellular thermal shift assay (CETSA) assay

HEK-293 cells were grown to 80%−90% confluence in 6-well plates under the above condition followed by BBR or DMSO treatment for 3 h. The cells were harvested and washed with PBS, and the suspension was incubated at each temperature point from 35 to 75 °C for 3 min. The samples were freeze-thaw 3 times and centrifuged at 20,000×*g* at 4 °C for 10 min. The 12 μL supernatant was mixed with 3 μL of 5 × loading buffer and then separated on a 10% SDS-PAGE for immunoblotting assay.

4.7. Recombinant EIF2AK2 expression

EIF2AK2 (258−551 residues, deletion 338−350 residues) with an N-terminal GST tag was cloned into PGEX-6P-1 vector and grown in *E. coli* Resetta2 (DE3) cells. The bacteria were grown at 37 °C for 4 h following induction with 0.5 mmol/L IPTG and continue cultured for at 18 °C 12 h. The protein was purified through GST beads and digested with HRV 3C enzyme. The protein was purified by size exclusion chromatography and the purity was checked *via* SDS-PAGE and Coomassie stain.

4.8. Surface plasmon resonance (SPR) analysis

The SPR assay was performed on a BIAcore T200 biosensor system (GE Healthcare Life Sciences, Piscataway, NJ, USA) at 25 °C using a CM5 chip. The bindings of EIF2AK2, VPS4B, eEF1A1 and PRDX3 at different concentrations of BBR were performed in 1 × PBS-P + (GE Healthcare Life Sciences) at a flow rate of 20 μL/min for 120 s. After each binding reaction, a further dissociation time of 60 s was applied after each injection to allow the signal to return to the baseline.

4.9. Molecular modeling analysis

An automated docking was carried out using the 3D structures of EIF2AK2 (PDB code: 2A19), eEF1A1 (PDB code: 6ZMO), PRDX3 (PDB code: 5UCX), VPS4B (PDB code: 7L9X) and Discovery Studio 4.5 software. The regularized protein was used in determination of the important amino acids in the predicted binding pocket. Interactive docking using Libdock protocol was carried out for all the conformers of BBR to the selected active site after energy minimization. The docked compound was assigned a score according to its binding mode onto the binding site.

4.10. Adeno-associated virus (AAV) knock down

The mice were transfected with adeno-associated virus (AAV-shEIF2KA2-GFP) to knock down EIF2AK2 (targeting sequence: 5′-GGAGTAGCCAT TACGTATAAA-3′) with adeno-associated virus expressing GFP (AAV-GFP) as a control. AAV-shEIF2KA2-GFP and AAV-GFP were purchased from Hanbio technology, China. Briefly, 100 μL of adeno-associated virus (10^{12} V·g/mL) were injected *via* tail vein.

4.11. LPS-induced mice acute inflammation

Animal experiments were approved by the Ethics Committee of the Institute of Medicinal Biotechnology, Chinese Academy of Medical Sciences and Peking Union Medical College, Beijing, China, with the approval number IBM20211102D201. Twelve-week-old male C57BL/6 mice were injected i.p. with BBR (3 mg/kg) or saline for twice every 24 h before i.p. injection of LPS (10 mg/kg). After 3 h, mice were sacrificed, and the blood and tissue were obtained and detected by ELISA or HE stain.

4.12. Statistical analyses

All values are expressed as the mean ± SD. Statistical analysis was performed with one-way ANOVA by SPSS 16.0 with all data points showing a normal distribution, $^{*}P < 0.05$, $^{**}P < 0.01$, $^{***}P < 0.001$. No exclusion of data points was used. The researchers were not blinded to the distribution of treatment groups when performing experiments and data assessment. Sample sizes were selected to ensure an adequate power based on the preliminary results.

Acknowledgments

This work was supported by the CAMS initiative for innovative medicine (2022-I2M-2-002, China) and National Natural Science Foundation of China (32141003).

Author contributions

Danqing Song, Jiandong Jiang and Yanxiang Wang conceived idea and designed experiments; Wei Wei, Xixi Guo and Tianyun Fan designed and synthesized the photoaffinity probes; Qingxuan Zeng and Xintong Zhang performed the probe screening experiments; Liping Zhao, Yan Wang and Yinghong Li overexpressed, purified

the proteins, and performed the CESTA and ITC experiments; Yonghua Liu and Hongbin Deng performed animal experiments.

Conflicts of interest

The authors declare no competing financial interests.

Appendix A. Supporting information

Supporting data to this article can be found online at https://doi.org/10.1016/j.apsb.2022.12.009.

References

1. Cicero AF, Baggioni A. Berberine and its role in chronic disease. *Adv Exp Med Biol* 2016;**928**:27–45.
2. Feng X, Sureda A, Jafari S, Memariani Z, Tewari D, Annunziata G, et al. Berberine in cardiovascular and metabolic diseases: from mechanisms to therapeutics. *Theranostics* 2019;**9**:1923–51.
3. Suadoni MT, Atherton I. Berberine for the treatment of hypertension: a systematic review. *Compl Ther Clin Pract* 2021;**42**:101287.
4. Wang K, Feng X, Chai L, Cao S, Qiu F. The metabolism of berberine and its contribution to the pharmacological effects. *Drug Metab Rev* 2017;**49**:139–57.
5. Gu C, Yin Z, Nie H, Liu Y, Yang J, Huang G, et al. Identification of berberine as a novel drug for the treatment of multiple myeloma *via* targeting UHRF1. *BMC Biol* 2020;**18**:33.
6. Kim N, Park J, Gadhe CG, Cho SJ, Oh Y, Kim D, et al. A protoberberine derivative HWY336 selectively inhibits MKK4 and MKK7 in mammalian cells: the importance of activation loop on selectivity. *PLoS One* 2014;**9**:e91037.
7. Ruan H, Zhan YY, Hou J, Xu B, Chen B, Tian Y, et al. Berberine binds RXRalpha to suppress beta-catenin signaling in colon cancer cells. *Oncogene* 2017;**36**:6906–18.
8. Subair TI, Soremekun OS, Olotu FA, Soliman MES. Prospecting the therapeutic edge of a novel compound (B12) over berberine in the selective targeting of retinoid X receptor in colon cancer. *J Mol Model* 2021;**27**:231.
9. Xu B, Jiang X, Xiong J, Lan J, Tian Y, Zhong L, et al. Structure–activity relationship study enables the discovery of a novel berberine analogue as the RXRalpha activator to inhibit colon cancer. *J Med Chem* 2020;**63**:5841–55.
10. Zeng Q, Deng H, Li Y, Fan T, Liu Y, Tang S, et al. Berberine directly targets the NEK7 protein to block the NEK7-NLRP3 interaction and exert anti-inflammatory activity. *J Med Chem* 2021;**64**:768–81.
11. Zeng QX, Wei W, Fan TY, Deng HB, Guo XX, Zhao LP, et al. Capture and identification of dual specificity mitogen-activated protein kinase kinase 7 as a direct proteomic target of berberine to affect the c-Jun N-terminal kinase pathway. *CCS Chemistry* 2022;**4**:1535–44.
12. Xu J, Li X, Ding K, Li Z. Applications of activity-based protein profiling (ABPP) and bioimaging in drug discovery. *Chem Asian J* 2020;**15**:34–41.
13. Martin-Acosta P, Meng Q, Klimek J, Reddy AP, David L, Petrie SK, et al. A clickable photoaffinity probe of betulinic acid identifies tropomyosin as a target. *Acta Pharm Sin B* 2022;**12**:2406–16.
14. Chen X, Wang Y, Ma N, Tian J, Shao Y, Zhu B, et al. Target identification of natural medicine with chemical proteomics approach: probe synthesis, target fishing and protein identification. *Signal Transduct Targeted Ther* 2020;**5**:72.
15. Zhao B, Liu N, Chen L, Geng S, Fan Z, Xing J. Direct label-free methods for identification of target proteins in agrochemicals. *Int J Biol Macromol* 2020;**164**:1475–83.
16. Ma X, Zhang T, Luo Z, Li X, Lin M, Li R, et al. Functional nanovector boost anti-atherosclerosis efficacy of berberine in Apoe$^{-/-}$ mice. *Acta Pharm Sin B* 2020;**10**:1769–83.
17. Liu J, Zhuang Y, Wu J, Wu Q, Liu M, Zhao Y, et al. IKKbeta mediates homeostatic function in inflammation *via* competitively phosphorylating AMPK and IkappaBalpha. *Acta Pharm Sin B* 2022;**12**:651–64.
18. Chen FL, Yang ZH, Liu Y, Li LX, Liang WC, Wang XC, et al. Berberine inhibits the expression of TNFalpha, MCP-1, and IL-6 in AcLDL-stimulated macrophages through PPARgamma pathway. *Endocrine* 2008;**33**:331–7.
19. Wang Y, Zhou X, Zhao D, Wang X, Gurley EC, Liu R, et al. Berberine inhibits free fatty acid and LPS-induced inflammation *via* modulating ER stress response in macrophages and hepatocytes. *PLoS One* 2020;**15**:e0232630.
20. Gong YN, Wang X, Wang J, Yang Z, Li S, Yang J, et al. Chemical probing reveals insights into the signaling mechanism of inflammasome activation. *Cell Res* 2010;**20**:1289–305.
21. Hill JR, Robertson AAB. Fishing for drug targets: a focus on diazirine photoaffinity probe synthesis. *J Med Chem* 2018;**61**:6945–63.
22. Lee W, Huang Z, Am Ende CW, Seneviratne U. Protocol for clickable photoaffinity labeling and quantitative chemical proteomics. *STAR Protoc* 2021;**2**:100593.
23. Chukwurah E, Farabaugh KT, Guan BJ, Ramakrishnan P, Hatzoglou M. A tale of two proteins: PACT and PKR and their roles in inflammation. *FEBS J* 2021.
24. Dhar A. The role of PKR as a potential target for treating cardiovascular diseases. *Curr Cardiol Rev* 2017;**13**:28–31.
25. Gal-Ben-Ari S, Barrera I, Ehrlich M, Rosenblum K. PKR: a kinase to remember. *Front Mol Neurosci* 2018;**11**:480.
26. Lan T, Tao A, Xu X, Kvietys P, Rui T. Peroxynitrite/PKR axis modulates the NLRP3 inflammasome of cardiac fibroblasts. *Front Immunol* 2020;**11**:558712.
27. Stunden HJ, Latz E. PKR stirs up inflammasomes. *Cell Res* 2013;**23**:168–70.
28. Duan J, Lang Y, Song C, Xiong J, Wang Y, Yan Y. siRNA targeting of PRDX3 enhances cisplatin induced apoptosis in ovarian cancer cells through the suppression of the NF kappaB signaling pathway. *Mol Med Rep* 2013;**7**:1688–94.
29. Elumalai S, Karunakaran U, Moon JS, Won KC. High glucose-induced PRDX3 acetylation contributes to glucotoxicity in pancreatic beta-cells: prevention by Teneligliptin. *Free Radic Biol Med* 2020;**160**:618–29.
30. Estin ML, Thompson SB, Traxinger B, Fisher MH, Friedman RS, Jacobelli J. Ena/VASP proteins regulate activated T-cell trafficking by promoting diapedesis during transendothelial migration. *Proc Natl Acad Sci U S A* 2017;**114**:E2901–10.
31. Futosi K, Fodor S, Mocsai A. Neutrophil cell surface receptors and their intracellular signal transduction pathways. *Int Immunopharm* 2013;**17**:638–50.
32. Kienes I, Bauer S, Gottschild C, Mirza N, Pfannstiel J, Schroder M, et al. DDX3X links NLRP11 to the regulation of type I interferon responses and NLRP3 inflammasome activation. *Front Immunol* 2021;**12**:653883.
33. Verma P, Sharma A, Sodhi M, Thakur K, Kataria RS, Niranjan SK, et al. Transcriptome analysis of circulating PBMCs to understand mechanism of high altitude adaptation in native cattle of ladakh region. *Sci Rep* 2018;**8**:7681.
34. Wei S, Wang D, Li H, Bi L, Deng J, Zhu G, et al. Fatty acylCoA synthetase FadD13 regulates proinflammatory cytokine secretion dependent on the NF-kappaB signalling pathway by binding to eEF1A1. *Cell Microbiol* 2019;**21**:e13090.
35. Xu L, Zhai L, Ge Q, Liu Z, Tao R. Vacuolar protein sorting 4B (VPS4B) regulates apoptosis of chondrocytes *via* p38 mitogen-activated protein kinases (MAPK) in osteoarthritis. *Inflammation* 2017;**40**:1924–32.
36. Zhang D, Wang L, Yan L, Miao X, Gong C, Xiao M, et al. Vacuolar protein sorting 4B regulates apoptosis of intestinal epithelial cells *via* p38 MAPK in Crohn's disease. *Exp Mol Pathol* 2015;**98**:55–64.
37. Fan T, Cheng Y, Wei W, Zeng Q, Guo X, Guo Z, et al. Palmatine derivatives as potential antiplatelet aggregation agents *via* protein kinase G/vasodilator-stimulated phosphoprotein and phosphatidylinositol 3-kinase/Akt phosphorylation. *J Med Chem* 2022;**65**:7399–413.

38. Lu B, Nakamura T, Inouye K, Li J, Tang Y, Lundback P, et al. Novel role of PKR in inflammasome activation and HMGB1 release. *Nature* 2012;**488**:670−4.
39. Taylor SS, Haste NM, Ghosh G. PKR and eIF2alpha: integration of kinase dimerization, activation, and substrate docking. *Cell* 2005;**122**: 823−5.
40. Dey M, Mann BR, Anshu A, Mannan MA. Activation of protein kinase PKR requires dimerization-induced *cis*-phosphorylation within the activation loop. *J Biol Chem* 2014;**289**:5747−57.
41. Sud N, Rutledge AC, Pan K, Su Q. Activation of the dsRNA-activated protein kinase PKR in mitochondrial dysfunction and inflammatory stress in metabolic syndrome. *Curr Pharm Des* 2016; **22**:2697−703.
42. Dey M, Cao C, Dar AC, Tamura T, Ozato K, Sicheri F, et al. Mechanistic link between PKR dimerization, autophosphorylation, and eIF2alpha substrate recognition. *Cell* 2005;**122**: 901−13.
43. Jiang W, Li S, Li X. Therapeutic potential of berberine against neurodegenerative diseases. *Sci China Life Sci* 2015;**58**:564−9.
44. Zhang W, Liu Y, Min Chin J, Phua KKL. Sustained release of PKR inhibitor C16 from mesoporous silica nanoparticles significantly enhances mRNA translation and anti-tumor vaccination. *Eur J Pharm Biopharm* 2021;**163**:179−87.
45. Hugon J, Mouton-Liger F, Dumurgier J, Paquet C. PKR involvement in Alzheimer's disease. *Alzheimer's Res Ther* 2017;**9**:83.
46. Hugon J, Paquet C. The PKR/P38/RIPK1 signaling pathway as a therapeutic target in Alzheimer's disease. *Int J Mol Sci* 2021:22.
47. Ju Hwang C, Choi DY, Park MH, Hong JT. NF-kappaB as a key mediator of brain inflammation in Alzheimer's disease. *CNS Neurol Disord: Drug Targets* 2019;**18**:3−10.
48. Yarza R, Vela S, Solas M, Ramirez MJ. c-Jun N-terminal kinase (JNK) signaling as a therapeutic target for Alzheimer's disease. *Front Pharmacol* 2015;**6**:321.
49. Sun Y, Xia M, Yan H, Han Y, Zhang F, Hu Z, et al. Berberine attenuates hepatic steatosis and enhances energy expenditure in mice by inducing autophagy and fibroblast growth factor 21. *Br J Pharmacol* 2018;**175**:374−87.
50. Li Y, Peng Z, Wang C, Li L, Leng Y, Chen R, et al. Novel role of PKR in palmitate-induced Sirt1 inactivation and endothelial cell senescence. *Am J Physiol Heart Circ Physiol* 2018;**315**:H571−80.
51. Fan AH, Zhao X, Liu H, Li D, Guo T, Zhang J, et al. eEF1A1 promotes colorectal cancer progression and predicts poor prognosis of patients. *Cancer Med* 2022. Available from: https://doi.org/10.1002/cam4.4848.
52. He Y, Zeng MY, Yang D, Motro B, Nunez G. NEK7 is an essential mediator of NLRP3 activation downstream of potassium efflux. *Nature* 2016;**530**:354−7.
53. Xu J, Lu L, Li L. NEK7: a novel promising therapy target for NLRP3-related inflammatory diseases. *Acta Biochim Biophys Sin* 2016;**48**:966−8.
54. Pei S, Ying J, Zhang Y, Su L, Cheng S, Ruan D. RhTSG-6 inhibits IL-1beta-induced extracellular matrix degradation and apoptosis by suppressing the p38, and JNK pathways in nucleus pulposus cells. *Folia Histochem Cytobiol* 2020;**58**:227−34.
55. Laczko R, Chang A, Watanabe L, Petelo M, Kahaleua K, Bingham JP, et al. *Inflammopharmacology* 2020;**28**:525−40.